Supplemental Material for

Perpendicular magnetic anisotropy in a single Dy adatom ferrimagnet.

COMPUTATIONAL DETAILS

The CF matrix $\Delta_{\rm CF}$ in Eq.(1) is obtained by projecting the self-consistent solutions of Eq.(3) into the $\{\phi_\gamma\}$ local f-shell basis, giving the "local Hamiltonian"

$$[H_{loc}]_{\gamma\gamma'} = \int_{\epsilon_b}^{\epsilon_t} {\rm d}\epsilon\, \epsilon [N(\epsilon)]_{\gamma\gamma'}$$
$$\approx \epsilon_0 \delta_{\gamma\gamma'} + \left[\xi \mathbf{l}\cdot\mathbf{s} + \Delta_{\rm CF} + \frac{\Delta_{\rm EX}}{2}\hat{\sigma}_z\right]_{\gamma\gamma'} + [V_U]_{\gamma\gamma'} ,$$

where $[N(\epsilon)]_{\gamma_1\gamma_2}$ is the f-projected density of states (fDOS) matrix

$$[N(\epsilon)]_{\gamma_1\gamma_2} = -\pi^{-1} {\rm Im}[G(z)_{\rm DFT+U}]_{\gamma_1\gamma_2} ,$$

ϵ_b is the bottom of the valence band, ϵ_t is the upper cut-off, which is naturally defined by the condition $\int_{\epsilon_b}^{\epsilon_t} {\rm d}\epsilon\, {\rm Tr}[N(\epsilon)] = 14$, and ϵ_0 is the mean position of the non-interacting $5f$ level. The matrix $\Delta_{\rm CF}$ is then obtained by removing the interacting DFT+U potential $[V_U]$, SOC $[\xi \mathbf{l}\cdot\mathbf{s}]$ and $\left[\frac{\Delta_{\rm EX}}{2}\hat{\sigma}_z\right]$ from H_{loc}.

The SOC parameter ξ is determined in a standard way,

$$\xi = \int_0^{R_{MT}} drr \frac{1}{2(Mc)^2}\frac{dV(r)}{dr}(u_l(r))^2 ,$$

by making use of the radial solutions u_l of the Kohn-Sham-Dirac scalar-relativistic equations [1], the relativistic mass $M = m + (E_l - V(r))/2c^2$ at an appropriate energy E_l, and the radial derivative of spherically-symmetric part of the DFT potential.

The $\Delta_{\rm EX}$ is calculated from the energy increase ΔE by flipping a direction of $4f$ spin moment M_S^{4f} in the simplified DFT+U calculations with the effective spherically symmetric Coulomb $U_{eff} = U - J = 6.2$ eV, J=0 [2]. These DFT+U calculations are analogous to the so-called "open core" approximation calculations in which the direction of M_S^{Dy} with respect to the M_S^{Ni} can be designated. The $\Delta_{\rm EX} = \Delta E/M_S^{Dy}$ of 11 meV is evaluated and used in the further DFT+U(HIA) calculations.

In the DFT+U(HIA) FP-LAPW calculations, 108 special k-points in the two-dimensional Brillouin zone were used, with Gaussian smearing for k-points weighting. The "muffin-tin" radii of $R_{MT} = 2.85$ *a.u.* for Dy, $R_{MT} = 2.20$ a.u. for Ni, $R_{MT} = 1.25$ a.u. for C were used. The LAPW basis cut-off is defined by the condition $R_{MT}^{Dy} \times K_{max} = 8.55$ (where K_{max} is the cut-off for LAPW basis set). The spin-orbit coupling (SOC) was included in a self-consistent second-variational procedure [3].

MAE FOR GR/NI(111) INTERFACE

We perform the supercell calculations for GR overlayer on the Ni(111) surface. A supercell slab model is shown in Fig. S1A which consists of a nine-layer Ni(111) substrate and GR monolayers on each side of the substrate. We consider the HCP (or "1-3") (one of the C-atoms is on the top of Ni surface, another is over the second Ni sub-surface ML) placement for graphene overlayer (GR/Ni$_9$/GR). The in-plane experimental Ni lattice constant of 4.7 a.u. was adopted and kept fixed in the calculations. The $d_{[C-Ni]}$= 3.875 a.u. [4] separation between the carbon atoms of graphene and the topmost Ni-layer is used. A vacuum region of 20 a.u. is employed in order to reduce the slab's replica interaction along the z-direction.

We make use of the relativistic version of the full-potential linearized augmented plane-wave method (FP-LAPW) [3], in which SOC is included in a self-consistent second-variational procedure. The conventional (von Barth-Hedin) local spin-density approximation (LSDA) is adopted in the calculations, which is expected to be valid for itinerant metallic systems. The radii of the atomic muffin-tin (MT) spheres are set to 1.25 a.u. for

C atoms, and 2.2 a.u. for Ni atoms. The parameter $R_{Ni} \times K_{max} = 7.7$ defines the basis set size and the two-dimensional Brillouin zone (BZ) was sampled with 225 k points.

Spin M_S and orbital M_L magnetic MT-sphere moments are shown in Tab. I for the graphene and Ni atom layers in GR/Ni_9/GR. The moments are practically zero for the C-atoms of graphene. There is a reduction of the M_S and M_L values for the surface Ni (Ni-S) layer, indicating the interaction with the C atom of graphene on the top. In addition, there is a sizeable M_S moment of -0.15 μ_B in the interstitial.

TABLE I: Spin (M_S) and orbital (M_L) magnetic moments in the MT-sphere of the graphene and Ni atom layers (in all calculations, the magnetization is directed along the z-axis along the surface normal.) The total, and layer-resolved $T(\theta = \frac{\pi}{4}, \phi = 0)$ for GR/Ni_9/GR.

Moments (μ_B)	Graphene	Ni-S	Ni-(S-1)	Ni-(S-2)	Ni-(S-3)	Ni-(S-4)
M_S	0.01	0.48	0.55	0.59	0.60	0.60
M_L	0.00	0.04	0.05	0.06	0.05	0.06
Torque (meV)	Total	Ni-S	Ni-(S-1)	Ni-(S-2)	Ni-(S-3)	Ni-(S-4)
$T(\theta = \frac{\pi}{4}, \phi = 0)$	0.18	0.25	0.03	-0.05	-0.07	0.02

We make use of the magnetic force theorem [6] to evaluate the uniaxial magnetic anisotropy (MAE) for GR/Ni_9/GR. The spin magnetic moment M_S is rotated, and a single energy band calculation is performed for the new orientation of M_S. The MAE results from SOC-induced changes in the band eigenvalues $E_A(\theta, \phi) = \sum_i^{occ} \epsilon_i(\theta, \phi)$. For a hexagonal symmetry, the magnetic anisotropic energy $E_A(\theta, \phi)$ as a function of the spherical angles θ and ϕ reads,

$$\begin{aligned} E_A(\theta, \phi) &= K_1 \sin^2\theta + K_2 \sin^4\theta + \\ & K_3 \sin^6\theta + K_4 \sin^6\theta \cos 6\phi \ , \end{aligned} \tag{1}$$

where, K_1 and K_2 are the uniaxial MAE constants, and K_3 and K_4 are the higher-order anisotropy constants [5].

In practice, it is more convenient to use the linear response theory, and evaluate the torque $T(\theta, \phi) = \partial E_A(\theta, \phi)/\partial\theta$ [7]. From the angular dependence of the torque,

$$\begin{aligned} T(\theta, \phi) &= K_1 \sin 2\theta + K_2 \sin 2\theta(1 - \cos 2\theta) + \\ & \frac{3}{4}(K_3 + K_4 \cos 6\phi) \sin 2\theta(1 - \cos 2\theta)^2 \ , \end{aligned} \tag{2}$$

the uniaxial MAE constants are evaluated. An advantage of this approach is that it allows separation of the Eq.(2) into the sum of the element-specific contributions from different atoms in the unit cell [7], and to evaluate the element-specific contributions to the anisotropy constants and the total MAE. We point out that care should be taken on the convergence of the $T(\theta, \phi)$ torque Eq.(2) with respect to the two-dimensional BZ integration. For GR/Ni_9/GR case, we found that the torque value convergence better than 0.1 meV is achieved for 1521 k-points in the 2D-BZ.

The θ angular dependence of $T(\theta, \phi)$ in Eq.(2) with $\phi = 0$ is shown in Fig. 1S for GR/Ni_9/GR unit cell. Note that the $T(\theta, \phi = \pi/2)$ angular dependence is found to be very similar. In what follows, we will neglect the sixth-order anisotropy constants K_3 and K_4, and consider only the K_1 and K_2 uniaxial anisotropies in Eq.(2). Fitting $T(\theta, \phi)$ angular dependence by Eq.(2), we obtain K_1 = 0.21 meV and K_2 = -0.03 meV per unit cell. The uniaxial MAE $= E_A[M||x] - E_A[M||z] (= K_1 + K_2) = 0.18$ meV per unit cell is evaluated. The positive MAE sign indicates the perpendicular magnetic anisotropy for GR/Ni_9/GR.

As follows from Eq.(2), the uniaxial MAE is equal to the value of $T(\theta = \frac{\pi}{4}, \phi = 0)$. The total, and layer-resolved $T(\theta = \frac{\pi}{4}, \phi = 0)$ for GR/Ni_9/GR unit cell are shown in Table S1. Note that for surface Ni (Ni-S), sub-surface Ni (Ni-(S-1)), Ni-(S-2), and Ni-(S-3) layers, these are twice the contributions from individual Ni layers in the unit cell. In Table S2, we show the layer-resolved contributions to the uniaxial MAE. The C atoms of graphene do not contribute to the total torque since their induced magnetic moments are small, and the SOC is weak. The surface Ni (Ni-S) layer contributes the most to the positive MAE. The MAE contribution from the Ni layers, which are away from the GR/Ni(111) interface is substantially smaller.

It is common to write the MAE of the ferromagnetic film as

$$\mathrm{MAE} = d \times K_V + 2K_I \ ,$$

where K_V is a "volume" and K_I is the GR/Ni_9/GR interface contributions.. Since we do not consider any strain in the Ni film, the K_V must go to zero. It is consistent with the layer-resolved MAE shown in Table S2.

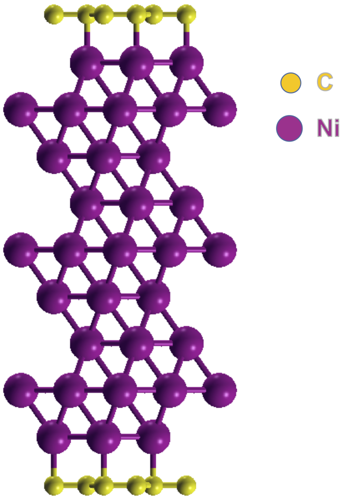

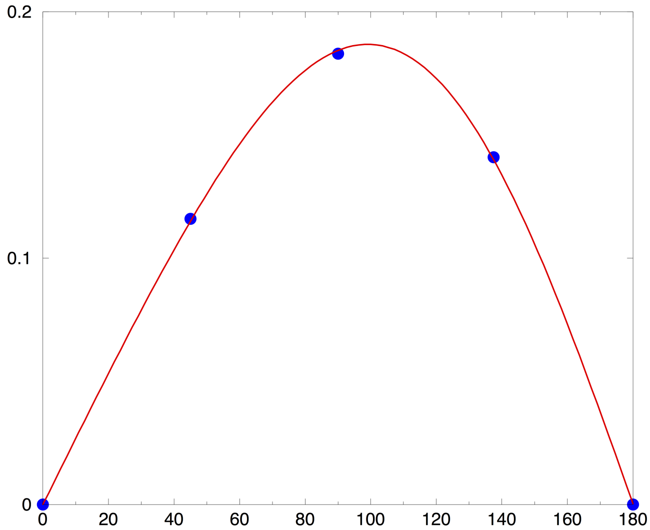

FIG. 1: A schematic crystal structure used to represent the GR/Ni_9/GR (A). The θ angular dependence of $T(\theta, \phi = 0)$ per unit cell (B).

TABLE II: The layer-resolved contributions to the MAE for GR/Ni_9/GR (meV).

MAE	GR	Ni-S	Ni-(S-1)	Ni-(S-2)	Ni-(S-3)	Ni-(S-4)
(meV)	0.0	0.12	0.02	-0.03	-0.03	0.02

Additional shape anisotropy (SAE) induced by the magnetic dipole-dipole interaction can be estimated using the relation SAE = -$2\pi M^2$ to the magnetisation density M (in CGS units). This additional negative SAE of ≈ -0.008 meV per atom [9] can reduce the positive MAE. Thus, the small and positive total magnetocrystalline and shape MAE of ≈ 0.11 meV is found for GR/Ni_9/GR. Recent XAS and XMCD measurements [8] show small positive MAE for the GR/Ni(111), in a qualitative agreement with our calculations.

[1] A. MacDonald, W. Pickett and D. Koelling , J. Phys. C: Solid State Phys. **13**, 2675 (1980).
[2] J. Ishizuka, S. Sumita, A. Daido, and Y. Yanese, Phys. Rev. Lett. **123**, 217001 (2019).
[3] A. B. Shick, D. L. Novikov, and A. J. Freeman, Phys. Rev. B 56, R14259 (1997).
[4] P. A. Khomyakov *et al.*, Phys. Rev. B 79 (2009) 195425.
[5] S. Chikazumi, *Physics of Ferromagnetism*, Oxford , Clarendon Press , Oxford University Press (1997), p. 655.
[6] A. I. Liechtenstein, M. Katsnelson, V. Antropov, and V. Gubanov, J. Magn. Magn. Mater **67**, 65 (1987).
[7] S. Khmelevskyi, A. B. Shick, and P. Mohn, Phys. Rev. B **83**, 224419 (2011).
[8] A. Barla *et al.*, ACS Nano 10, 1101 (2016).
[9] F. Maca, A. B. Shick, J. Redinger, R. Podloucky, P. Weinberger, Chechoslovak J. of Phys. **53**, 33 (2003).